Electronic Supplementary Information

Anion triggered metallogel: demetalation, crystal growth inside gel matrix and improvement of viscoelastic properties using Au-NPs

Arnab Biswas, Mrigendra Dubey, Sujay Mukhopadhyay, Ashish Kumar and Daya Shankar Pandey*

Department of Chemistry, Faculty of Science, Banaras Hindu University, Varanasi-221 005, U.P., India

---

General Information:

Materials and Methods. Metal nitrates, common reagents and solvents were purchased from Merck, Qualigens or *s.d. fine-chem*. Ltd, Mumbai, India. The solvents were dried and distilled following standard procedures prior to their use. Propargyl bromide, 2-/ 4-hydroxybenzaldehyde, 2-acetylpyridine and $AuBr_3$ were purchased from Sigma Aldrich Chemical Co., USA and used as received.

^1H NMR spectra were obtained on a JEOL AL 300 FT–NMR spectrometer at room temperature using tetramethylsilane [$Si(CH_3)_4$] as an internal reference, whereas, ^1H NMR titrations were performed on a Bruker Advance 400 MHz. ESI-MS were obtained on Agilent 6520 Q-Tof mass spectrometer with a capillary voltage of 2.6–3.2 kV. Electronic absorption and emission spectra were obtained on Shimadzu UV-1601 and Perkin Elmer *LS* 55 spectrophotometers, respectively. The life-time measurements were made using a TCSPC system from Horiba Yovin (Model: Fluorocube- 01-NL). The samples were excited at 343 nm using a pico-second diode laser (Model: Pico Brite-375L). The data analysis was performed using IBH DAS (version 6, HORIBA Scientific, Edison, NJ) decay analysis software. Atomic force microscopic (AFM) images were captured using a NTMDT Solver NEXT Russia. Scanning electron microscopy (SEM) and Energy-dispersive X-ray spectroscopy (EDS) were performed on a Philips–FEI XL-30 ESEM TMP, Netherland. Transmission electron microscopic (TEM) analyses have been performed on a JEOL JEM 2100 HR Microscope with operating voltage 200 KV. Single Crystal X-Ray Diffraction (SCXRD) data were collected on a Bruker D-8 Venture X-ray diffractometer using Mo-Kα X-ray source at 100K. Structures were solved by direct methods (SHELXS 97) and refined by full-matrix least squares on F2 (SHELX 97)[1]. All the non-H atoms were treated anisotropically. The H-atoms attached to carbon were included as fixed contribution and geometrically calculated and refined using SHELX riding model. Computer program PLATON was used for analyzing the interaction and stacking distances[2]. Crystallographic data have been deposited with Cambridge Crystallographic Data Centre: **CCDC 1024772**. Quantum chemical calculations performed using a hybrid version of DFT and Hartree-Fock (HF) methods namely the B3LYP[3], wherein exchange energy from Becke's exchange functional is combined with exact energy from Hartree-Fock theory. Basis set 6-31G** used for C, H, N, and O which combines quasi-relativistic effective core potentials with a valence double basis-set[4] whereas LanL2DZ for the metal (Zn^{2+}). Geometry optimization and frequency calculations (to verify genuine minimum energy structure) were performed by Gaussian 09 programme[5].

Rheological Experimental Details: Measurements were performed using a stress-controlled Rheometer (Anton Paar Quality Control Rheometer RheolabQC instrument) equipped with stainless steel parallel plates (20 mm diameter, 0.2 mm gap between plates). Experiments were carried out on freshly prepared gels (1.1 %w/v). Linear viscoelastic regions of the samples were determined by measuring the storage modulus, G' (associated with energy storage), and the loss modulus G" (associated with the loss of energy) as a function of the stress amplitude. Dynamic oscillatory work was kept at a frequency of 1 rad s^{-1}. The following tests were performed: increasing amplitude of oscillation up to 100% apparent strain on shear, time and frequency sweeps at 22 °C (20 min and from 0.1 to 10 rad s^{-1}, respectively), and a heating run to 100 °C at a scan rate of 5 °C min^{-1}. All these measurements were conducted in triplicate.

Synthesis: Aldehydes 2-(prop-2-yn-1-yloxy)benzaldehyde [A-1] and 4-(prop-2-yn-1-yloxy)benzaldehyde [A-2] have been synthesized by simple propargylation of the 2-hdroxybenzaldehyde and 4-hydroxybenzaldehyde, respectively.

General procedure for syntheses of ligands. To a methanolic solution (30 mL) of the respective aldehydes (0.318 g, 2.0 mM) NaOH (0.08 g, 2.0 mM, 1 equiv) was added and the contents of the vessel stirred for 30 min at room temperature. Then 0.5 mL (4.0 mM) of 2-acetylpyridine and 12.0 mL of ammonia solution were added to the resulting solution successively. The reaction vessel was stoppered well and left for stirring at room temperature for another 48 hrs. Gradual precipitation observed over the said time and ensuing product was filtered off and washed with water several times.

TRPA-1. (Yield: 530 mg, 73%) *CHN Analysis* for $C_{24}H_{17}N_3O$; Found: C, 80.02; H, 4.92; N, 11.33; (Calculated: C, 79.32; H, 4.72; N, 11.56). *^{1}H NMR Spectra* (300 MHz, DMSO-d_6, δ ppm); 8.67 (m, 4H, Ar), 8.55 (s, 2H, Ar), 8.01 (m, 2H, Ar), 7.50 (d, 4H, Ar), 7.30 (d, 1H, Ar), 7.18 (d, 1H, Ar), 4.89 (s, 2H), 3.54 (s, 1H). *ESI-Mass Spectra* $[M+H]^+$, 364.1443 (Calc. 364.1450) (Figures S1 and S4)

TRPA-2. (Yield: 498 mg, 69%) *CHN Analysis* for $C_{24}H_{17}N_3O$; Found: C, 79.93; H, 4.98; N, 11.24; (Calculated: C, 79.32; H, 4.72; N, 11.56). *^{1}H NMR Spectra* (300 MHz, DMSO-d_6, δ ppm); 8.74 (d, 2H, Ar), 8.64 (d, 4H, Ar), 8.01 (m, 2H, Ar), 7.89 (d, 2H, Ar), 7.50 (m, 2H, Ar), 7.18 (d, 2H, Ar), 4.90 (s, 2H), 3.62 (s, 1H). *ESI-Mass Spectra* $[M+H]^+$, 364.1445 (Calc. 364.1450). (Figures S1 and S4)

General procedure for syntheses of complexes. Hydrated metal salts [$M(NO_3)_2 \cdot xH_2O$, 0.6 mM] were added to a solution of the ligand (182 mg, 0.5 mM) dissolved in 20 mL of methanol and resulting mixture stirred at room temperature for ~4 hrs. It was filtered to remove any solid impurities and the filtrate evaporated completely under reduced pressure. Residue thus obtained was washed thoroughly with water to remove excess of the metal salt.

Ni-TRPA-2. (Yield: 346 mg, 63.5%) *CHN Analysis* for $C_{24}H_{17}N_5NiO_7$; Found: C, 52.97; H, 3.54; N, 12.37; (Calculated: C, 52.78; H, 3.14; N, 12.82). *ESI-Mass Spectra* $[(TRPA\text{-}2) + Ni^{2+} + (NO_3^-)]^+$, 482.9819 (Calc. 483.0603) (Figure S6)

Cu-TRPA-2. (Yield: 303 mg, 55.1%) *CHN Analysis* for $C_{24}H_{17}CuN_5O_7$; Found: C, 53.13; H, 3.62; N, 12.34; (Calculated: C, 52.32; H, 3.11; N, 12.71). *ESI-Mass Spectra* $[(TRPA\text{-}2) + Cu^{2+} + (NO_3^-)]^+$, 488.1141 (Calc. 488.0546) (Figure S6)

Zn-TRPA-2. (Yield: 367 mg, 66.6%) *CHN Analysis* for $C_{24}H_{17}N_5O_7Zn$; Found: C, 52.67; H, 3.48; N, 12.23; (Calculated: C, 52.14; H, 3.10; N, 12.67). *^{1}H NMR Spectra* (300 MHz, DMSO-d_6, δ ppm); 9.34 (s, 2H, Ar), 9.13 (d, 2H, Ar), 8.44(d, 2H, Ar), 8.27 (s, 2H, Ar), 7.92 (s, 2H, Ar), 7.49 (s, 2H, Ar), 7.35 (s, 2H, Ar), 5.02 (s, 2H), 3.68 (s, 1H). *ESI-Mass Spectra* $[(C_{24}H_{17}N_3O) + Zn^{2+} + (NO_3^-)]^+$, 489.0772 (Calc. 489.0541) (Figures S2 and S5)

Cd-TRPA-2. (Yield: 342 mg, 56.9%) *CHN Analysis* for $C_{24}H_{17}CdN_5O_7$; Found: C, 48.57; H, 3.08; N, 11.32; (Calculated: C, 48.06; H, 2.86; N, 11.68). *^{1}H NMR Spectra* (300 MHz, DMSO-d_6, δ ppm); 9.05 (s, 4H, Ar), 8.66 (s, 2H, Ar), 8.32(d, 4H, Ar), 7.82 (s, 2H, Ar), 7.28 (s, 2H, Ar), 4.97 (s, 2H), 3.66 (s, 1H). *ESI-Mass Spectra* $[(C_{24}H_{17}N_3O) + Cd^{2+} + (NO_3^-)]^+$, 539.1036 (Calc. 539.0283); $[(C_{24}H_{17}N_3O) + Cd^{2+} + (NO_3^-)]^+$, 902.3351 (Calc. 902.1655) (Figure S7)

Hg-TRPA-2. (Yield: 360 mg, 52.3%) *CHN Analysis* for $C_{24}H_{17}HgN_5O_7$; Found: C, 42.33; H, 2.87; N, 10.03; (Calculated: C, 41.90; H, 2.49; N, 10.18). We were unable to procure ^{1}H NMR or ESI-MS data due to poor solubility of the complex in common solvents like $CHCl_3$/MeOH/-CH_3CN/H_2O/DMSO etc.

Zn-TRPA-1. (Yield: 354 mg, 64.2%) *CHN Analysis* for $C_{24}H_{17}N_5O_7Zn$; Found: C, 52.62; H, 3.51; N, 12.23; (Calculated: C, 52.14; H, 3.10; N, 12.67). *^{1}H NMR Spectra* (300 MHz, DMSO-d_6, δ ppm); 9.20 (d, 2H, Ar), 8.89 (s, 2H, Ar), 8.24 (m, 2H, Ar), 7.91 (d, 3H, Ar) 7.63 (s, 1H, Ar), 7.47 (s, 4H, Ar), 5.04 (s, 2H), 3.67 (s, 1H). *ESI-Mass Spectra* $[(C_{24}H_{17}N_3O) + Zn^{2+} + (NO_3^-)]^+$, 489.2319 (Calc. 489.0541) (Figures S2 and S5)

Metallogel ZTP2G. It was prepared by slow addition 0.6mL of HCl (0.25M, 7.5 equiv.) to a methanolic solution (1.0mL) of Zn-TRPA-2 (0.011 g, 2×10^{-2} M) keeping the resulting solution undisturbed for 5-10 min (gelation occurs at the same ratio of solution and acid with any volume). The gelation was affirmed by inverted vial method. *CHN Analysis* for $C_{24}H_{17}N_5O_7Zn$; Found: C, 52.64; H, 3.52; N, 12.21; (Calculated: C, 52.14; H, 3.10; N, 12.67). *ESI-Mass spectra* $[(C_{24}H_{17}N_3O) + H^+]^+$, 364.1435 (Calc. 364.1450); $[(C_{24}H_{17}N_3O) + CH_3OH]$, 395.0947 (Calc. 395.1634); $[(C_{24}H_{17}N_3O) + Zn^{2+} + Cl^-]^+$, 462.0363 (Calc. 462.0352); $[(C_{24}H_{17}N_3O) + 2HCl + 2H_2O + H^+]^+$, 472.0639 (Calc. 472.1195); $[2(C_{24}H_{17}N_3O) + H_2O]$, 744.3062 (Calc. 744.2849); $[2(C_{24}H_{17}N_3O) + 2\ CH_3OH + HCl]$, 827.1722 (Calc. 827.3113). (Figure S8)

Demetalated crystal from Zn-TRPA-2 (NA-TRPA-2). To a methanolic solution (1.0 mL) of Zn-TRPA-2 (0.011 g; 2×10^{-2} M) HNO_3 (0.22 mL; 0.9 M; 10 equiv.) was added and resulting solution was kept undisturbed for 48 h to obtain light yellowish needle shaped crystals. *CHN Analysis* for $C_{24}H_{18}N_4O_4$; Found: C, 67.78; H, 4.43; N, 12.98; (Calculated: C, 67.60; H, 4.25; N, 13.14). *ESI-Mass spectra* $[(C_{24}H_{17}N_3O) + H^+]^+$, 364.1435 (Calc. 364.1450); $[(C_{24}H_{17}N_3O) + CH_3OH]$, 395.0947 (Calc. 395.1634); $[Zn^{2+} + 2NO_3^- + 4CH_3OH + 5H_2O]$, 406.0923 (Calc. 406.0625); $[(C_{24}H_{17}N_3O) + HNO_3 + CH_3OH + H_2O]$, 476.0740 (Calc. 476.1696); $[2(C_{24}H_{17}N_3O) + 2HNO_3]$, 852.1907 (Calc. 852.2656) (Figure S9)

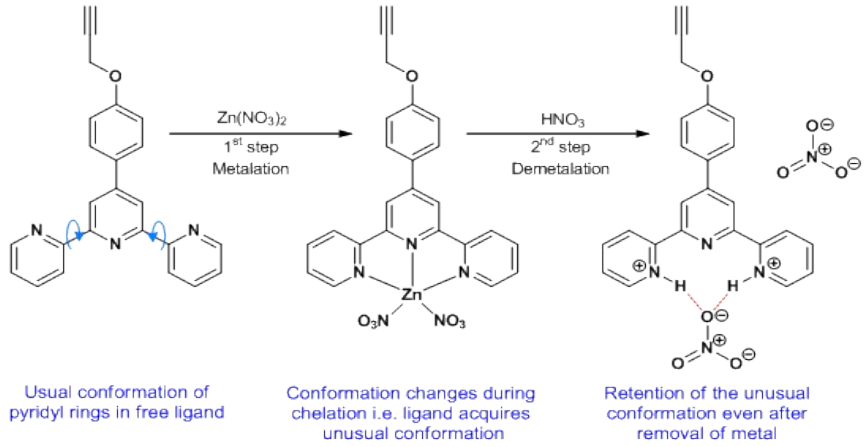

Scheme S1. Schematic representation for metalation and demetalation showing retention of conformation regarding terpyridyl unit of TRPA-2 in the demetalated species (NA-TRPA-2) even after demetalation of Zn-TRPA-2

Simultaneous Gelation and Demetalation. A glass vial containing 0.011 g (2×10^{-2} M) of Zn-TRPA-2 dissolved in 1.0 mL methanol was treated with a mixture of HCl (0.6 mL; 0.25 M) and HNO_3 (0.22 mL; 0.9M) drop wise and mixed properly. Resulting solution was kept undisturbed for 120 h. It afforded macroscopic fibres and light yellowish needle shaped crystals. *CHN Analysis* for gel part ($C_{24}H_{17}N_5O_7Zn$); Found: C, 52.73; H, 3.46; N, 12.33; (Calculated: C, 52.14; H, 3.10; N, 12.67). *CHN Analysis* for crystalline part ($C_{24}H_{18}N_4O_4$); Found: C, 67.84; H, 4.49; N, 12.87; (Calculated: C, 67.60; H, 4.25; N, 13.14). *ESI-Mass spectra* $[(C_{24}H_{17}N_3O) + H^+]^+$, 364.1435 (Calc. 364.1450); $[(C_{24}H_{17}N_3O) + CH_3OH]$, 395.0947 (Calc. 395.1634); $[(C_{24}H_{17}N_3O) + Zn^{2+} + Cl^-]^+$, 462.0363 (Calc. 462.0352); $[(C_{24}H_{17}N_3O) + 2HCl + 2H_2O + H^+]^+$, 472.0639 (Calc. 472.1195); $[(C_{24}H_{17}N_3O) + Zn^{2+} + HNO_3 + CH_3OH + H_2O]^{2+}$, 540.0987 (Calc. 540.0542); $[2(C_{24}H_{17}N_3O) + 2\ CH_3OH + HCl]$, 827.1722 (Calc. 827.3113); $[2(C_{24}H_{17}N_3O) + 2HNO_3]$, 852.1907 (Calc. 852.2656). (Figure S10)

Synthesis of Zn-TRPA-2 Capped Ag-NPs. To a solution of Zn-TRPA-2 (1.0 mL; 2×10^{-2} M; MeOH) 0.05 mL of 10^{-1} M methanolic $AgNO_3$ along with little amount of $NaBH_4$ dissolved in the same solvent was added. The capping agent/nanoparticle ratio was maintained 4:1 to avoid aggregations.

Synthesis of Zn-TRPA-2 Capped Au-NPs. To a solution of Zn-TRPA-2 (1.0 mL; 2×10^{-2} M; MeOH) in a glass vial 0.05 mL of 10^{-1} M methanolic $AuBr_3$ was added followed by a little amount of $NaBH_4$ dissolved in methanol. The capping agent/nanoparticle ratio was maintained 4:1 to avoid aggregations.

Gelation Procedure for GNZTP2G. To 1.0 mL freshly prepared Au-NPs solution 0.6mL of 0.25M HCl was added slowly and kept undisturbed for 30 min. After that, gelation was confirmed by inverted vial method.

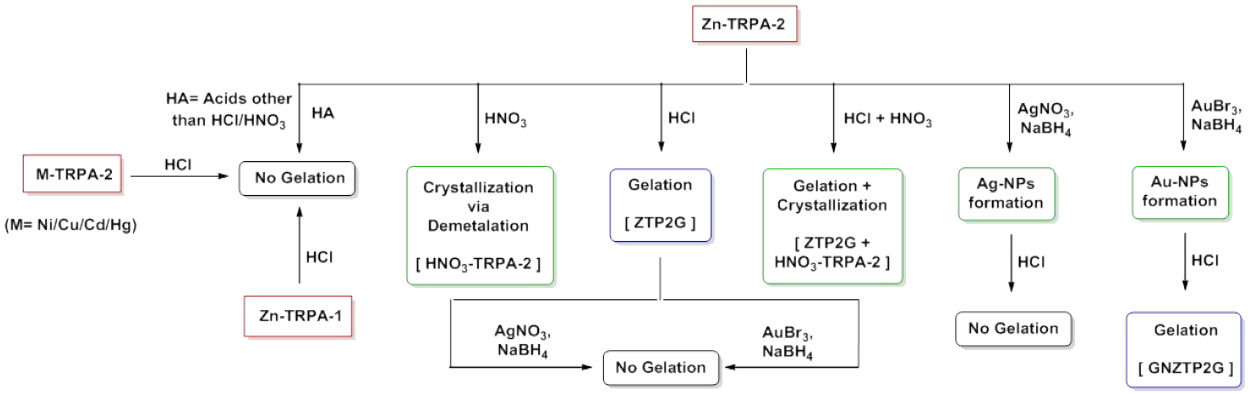

Scheme S2 Schematic overview showing all the trials for gelation with all complexes (M-TRPA-1/2)

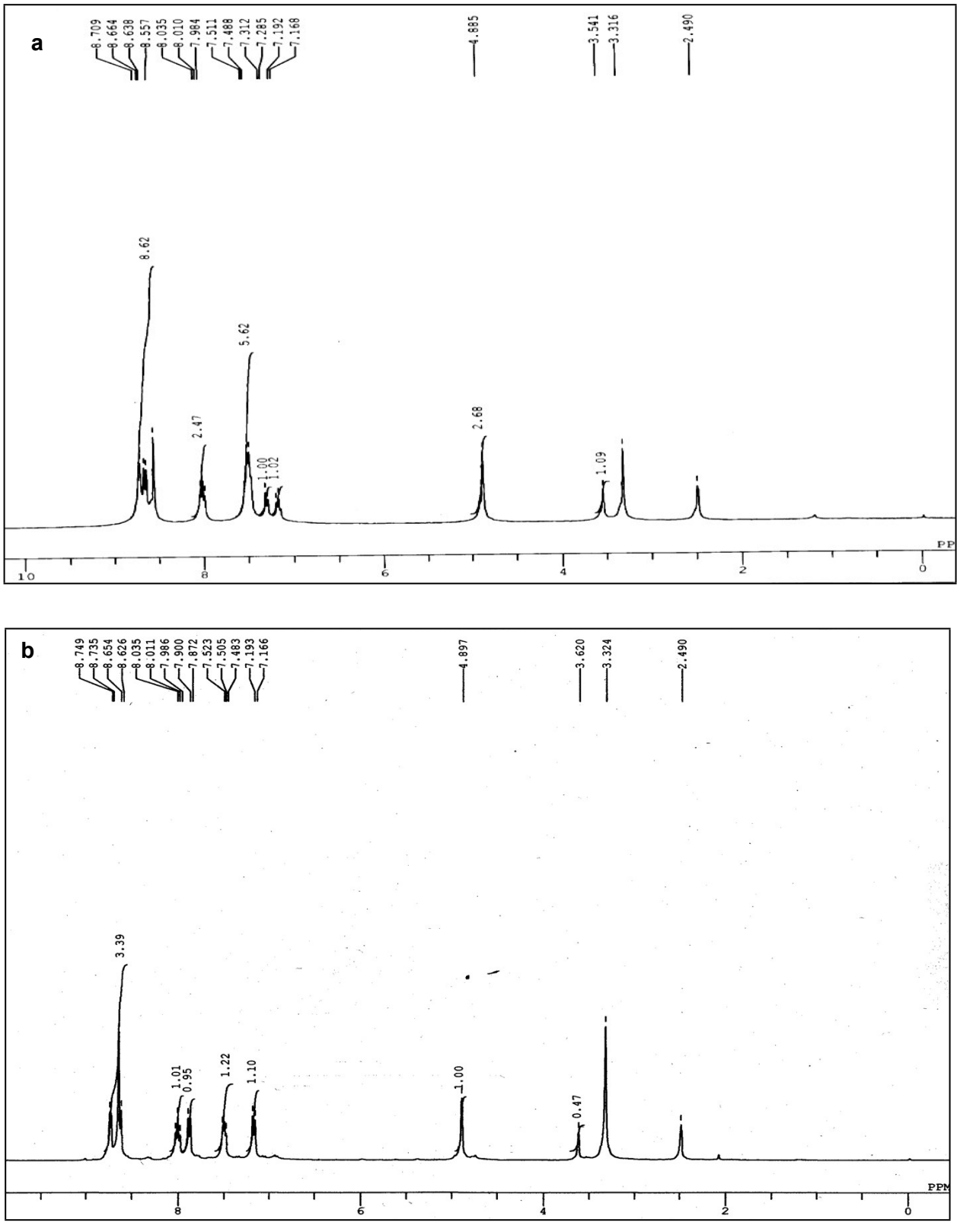

Figure S1. ^{1}H NMR spectra of ligands (a) TRPA-1 and (b) TRPA-2

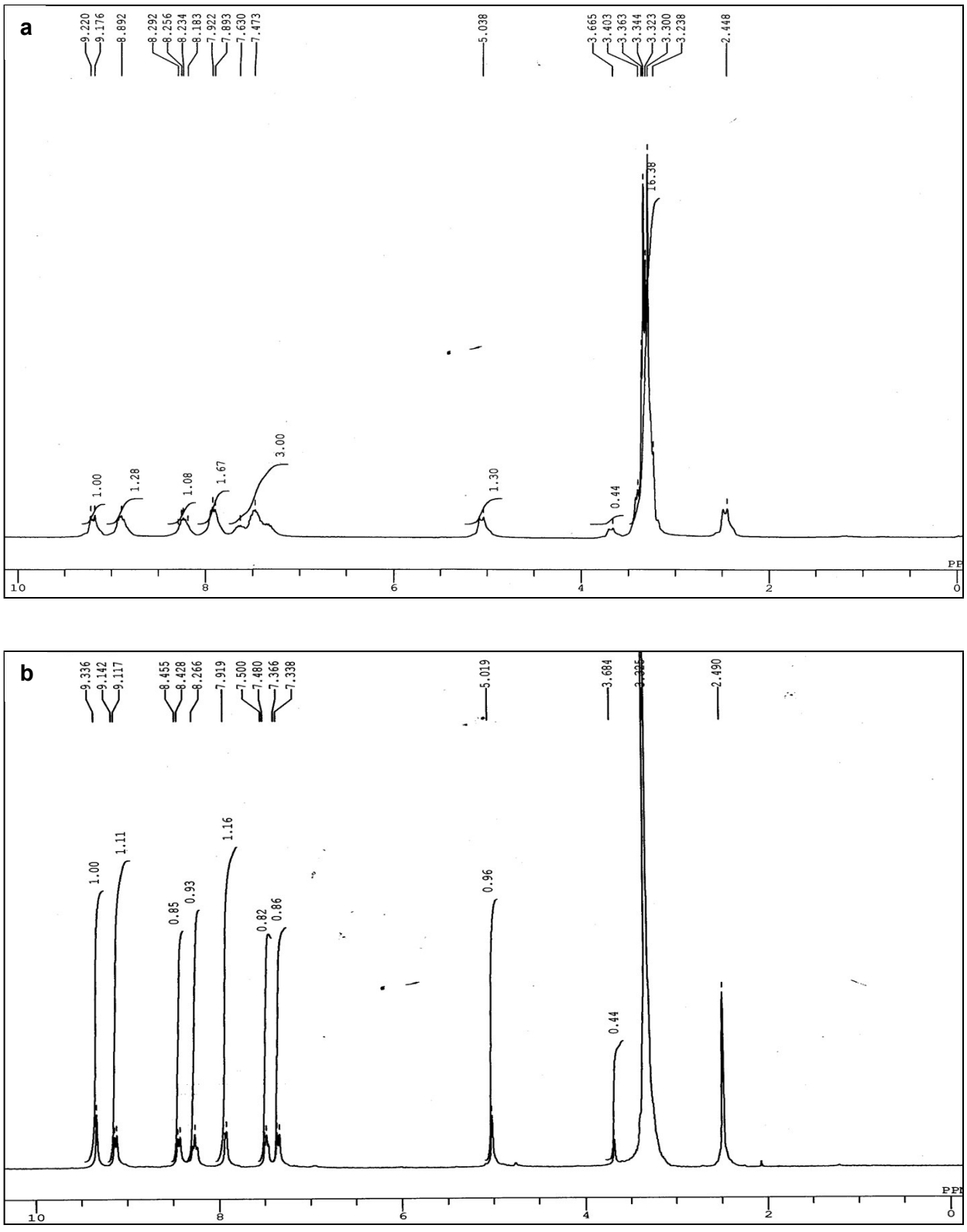

Figure S2. ^{1}H NMR spectra of (a) Zn-TRPA-1 and (b) Zn-TRPA-2

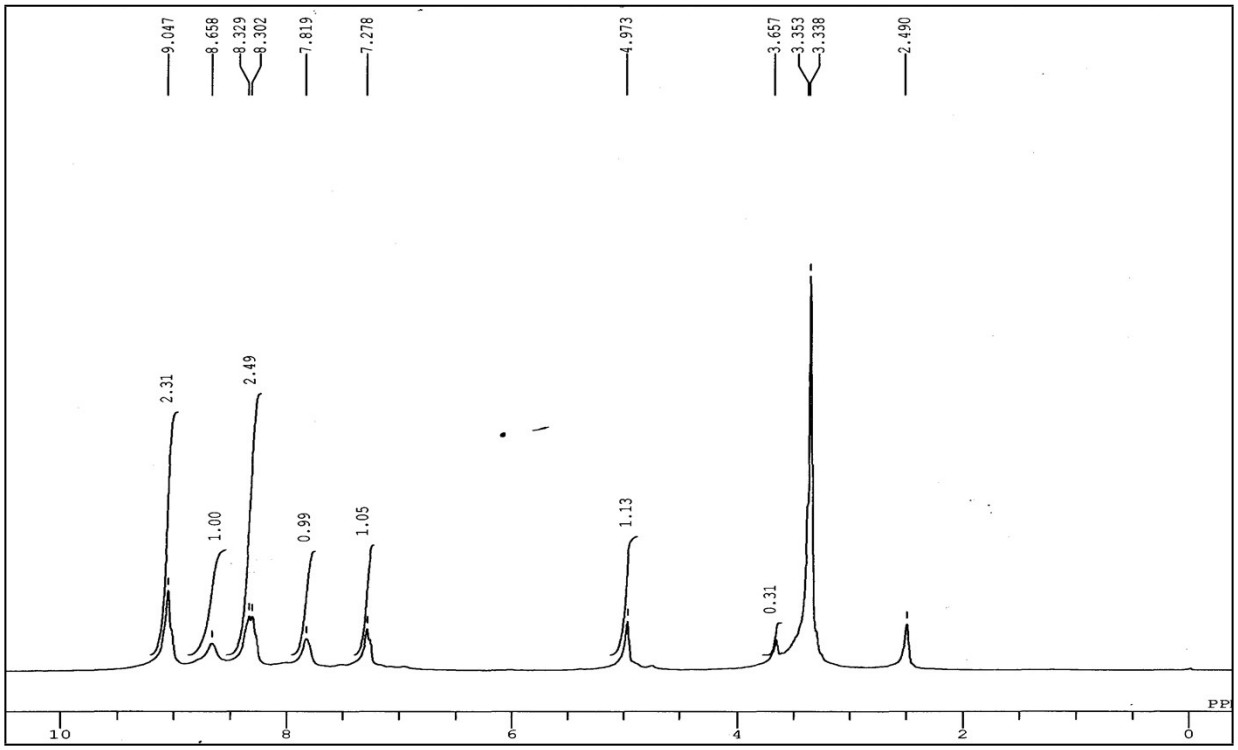

Figure S3. ^{1}H NMR spectra of Cd-TRPA-2 showing insignificant downfield shifts than in Zn-TRPA-2 and it is evident that metal induced 'intra-ligand charge transfer' (ICT) is maximum for Zn-TRPA-2 related to other metal complexes of TRPA-2 as well as Zn-TRPA-1

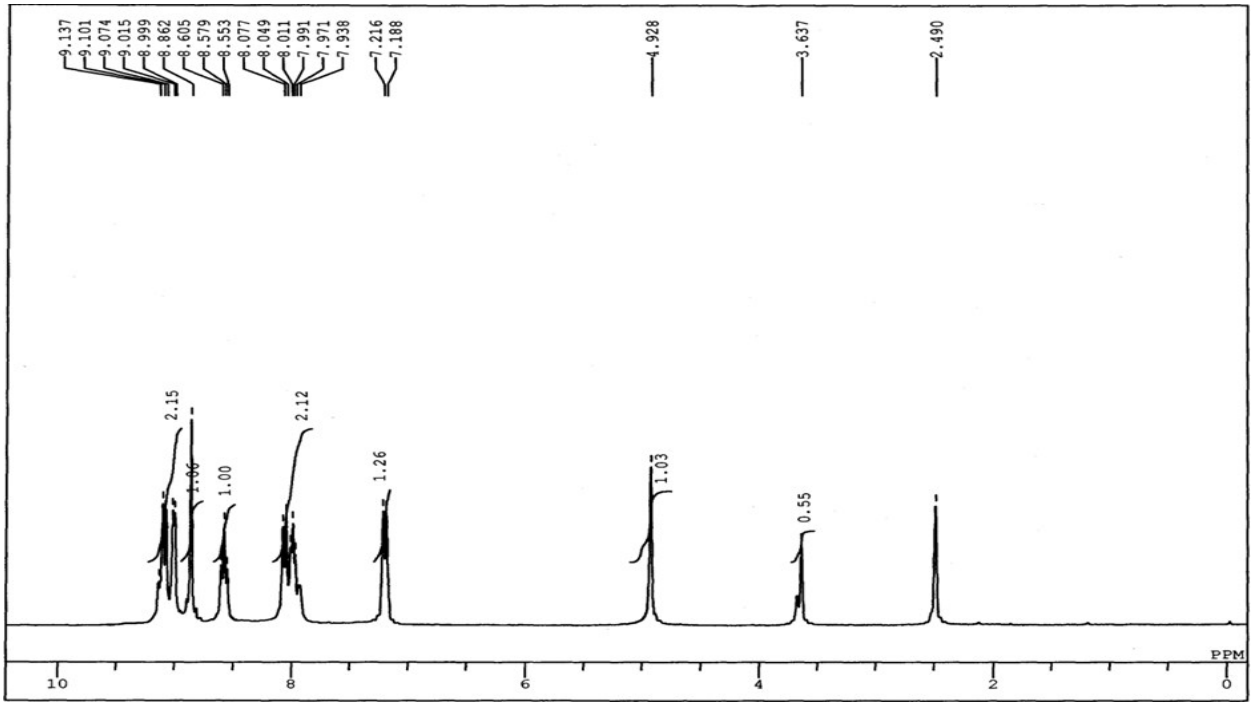

Figure S4. ^{1}HNMR spectra of NA-TRPA-2; it is clear from the spectra that terpyridyl core protons got a large downfield shift than those in free ligand TRPA-2 (Figure S1b) due to double protonation.

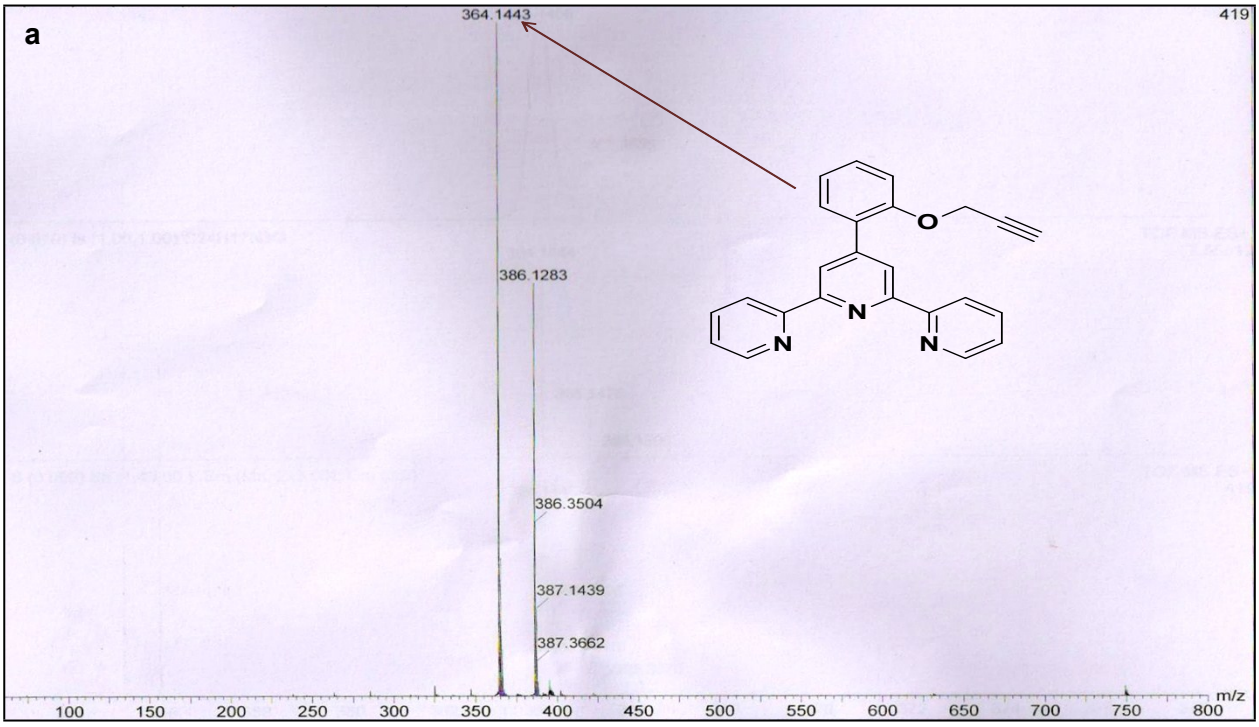
a
364.1443
419
386.1283
386.3504
387.1439
387.3662
m/z
100 150 200 250 300 350 400 450 500 550 600 650 700 750 800
O
N
N
N

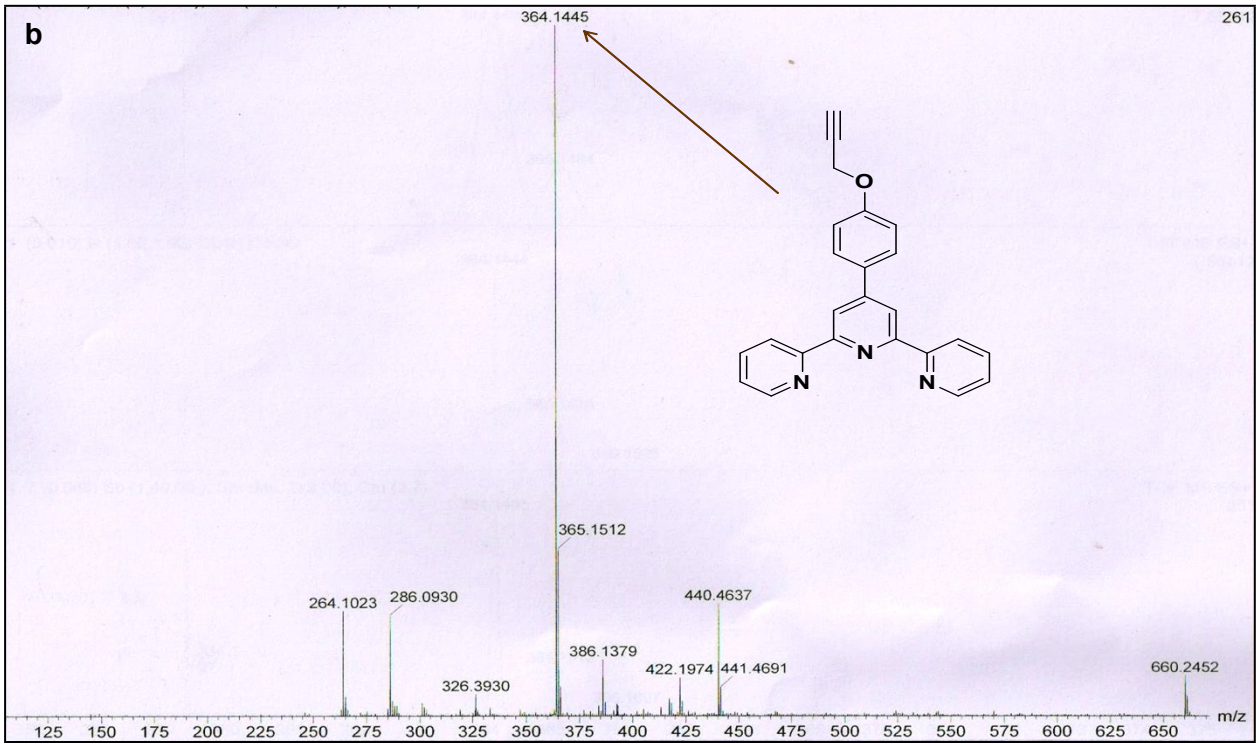
b
364.1445
261
365.1512
264.1023
286.0930
440.4637
386.1379
422.1974
441.4691
326.3930
660.2452
m/z
125 150 175 200 225 250 275 300 325 350 375 400 425 450 475 500 525 550 575 600 625 650
O
N
N
N

Figure S5. ESI-Mass spectra for the isomeric ligands (a) TRPA-1 and (b) TRPA-2

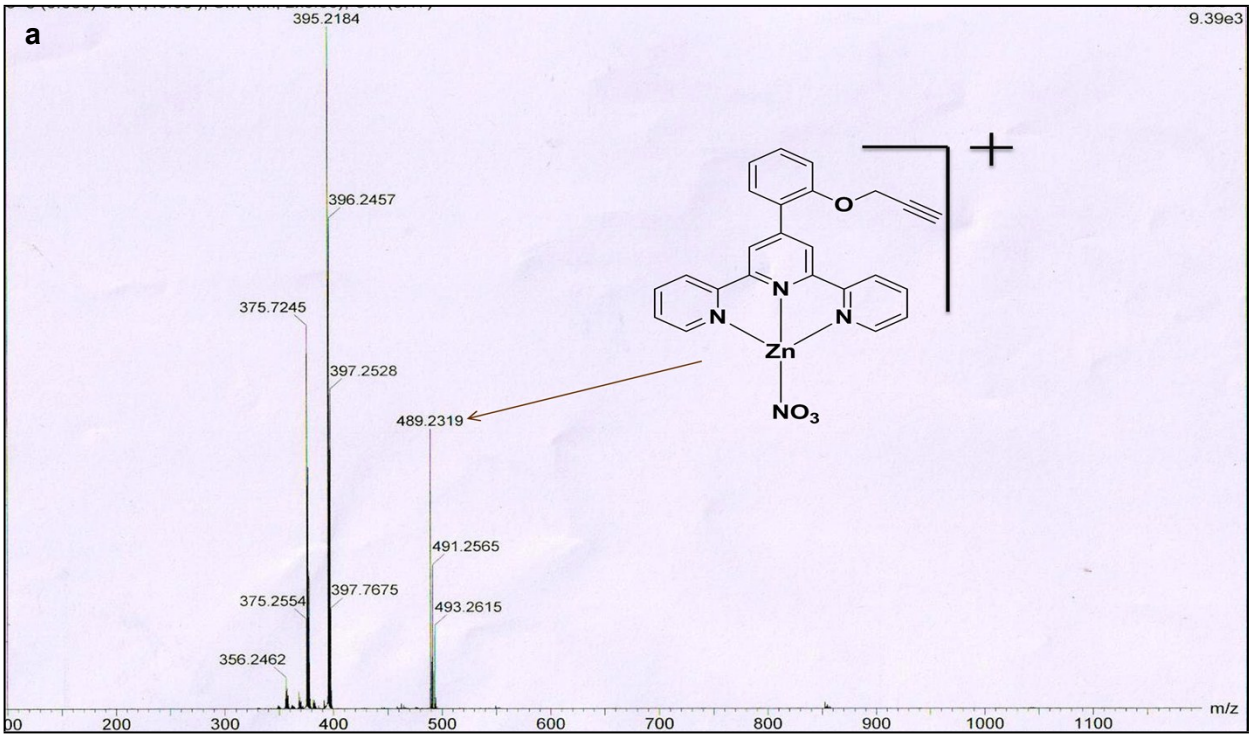

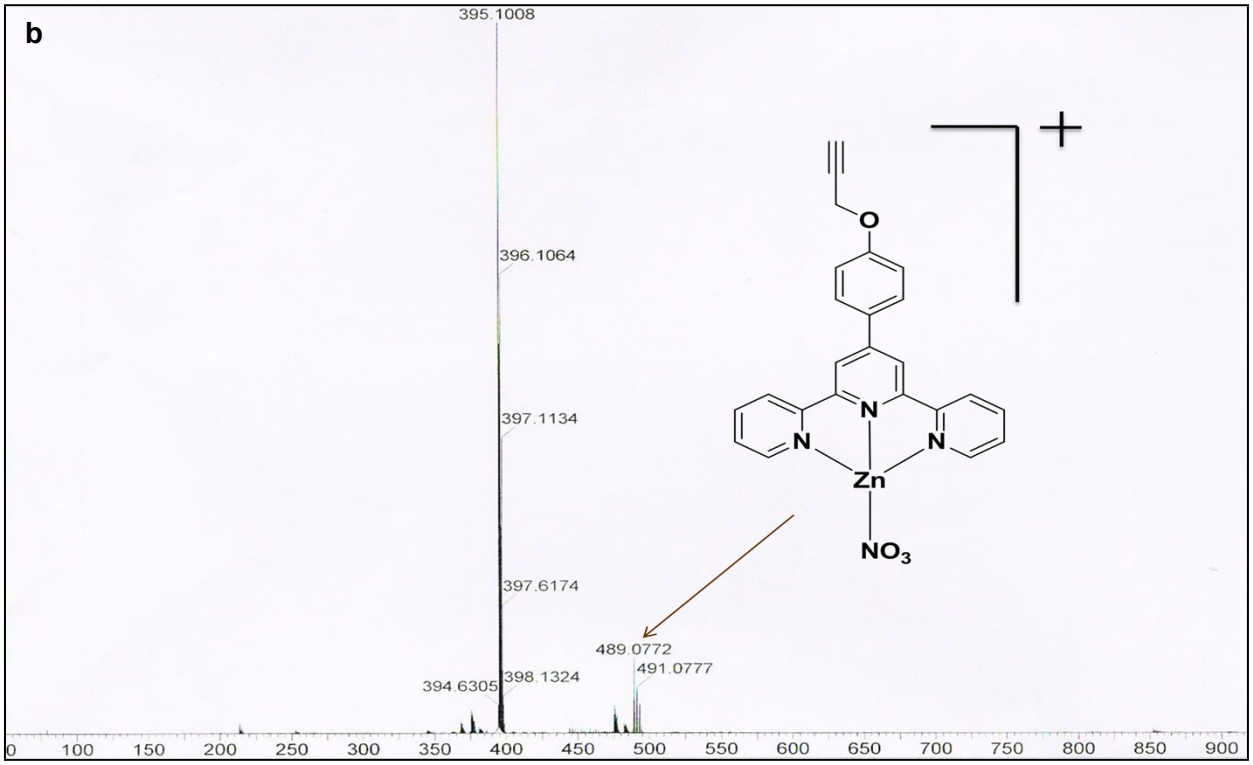

Figure S6. ESI- Mass spectra of (a) Zn-TRPA-1 and (b) Zn-TRPA-2

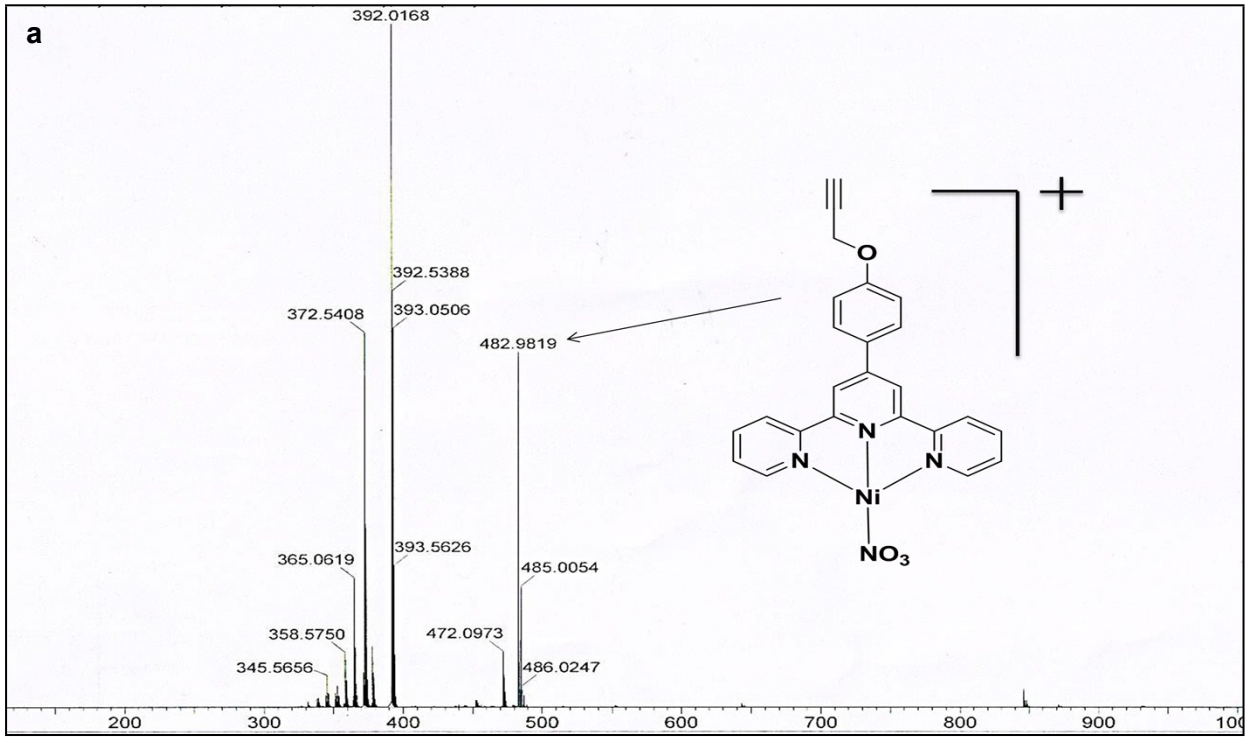

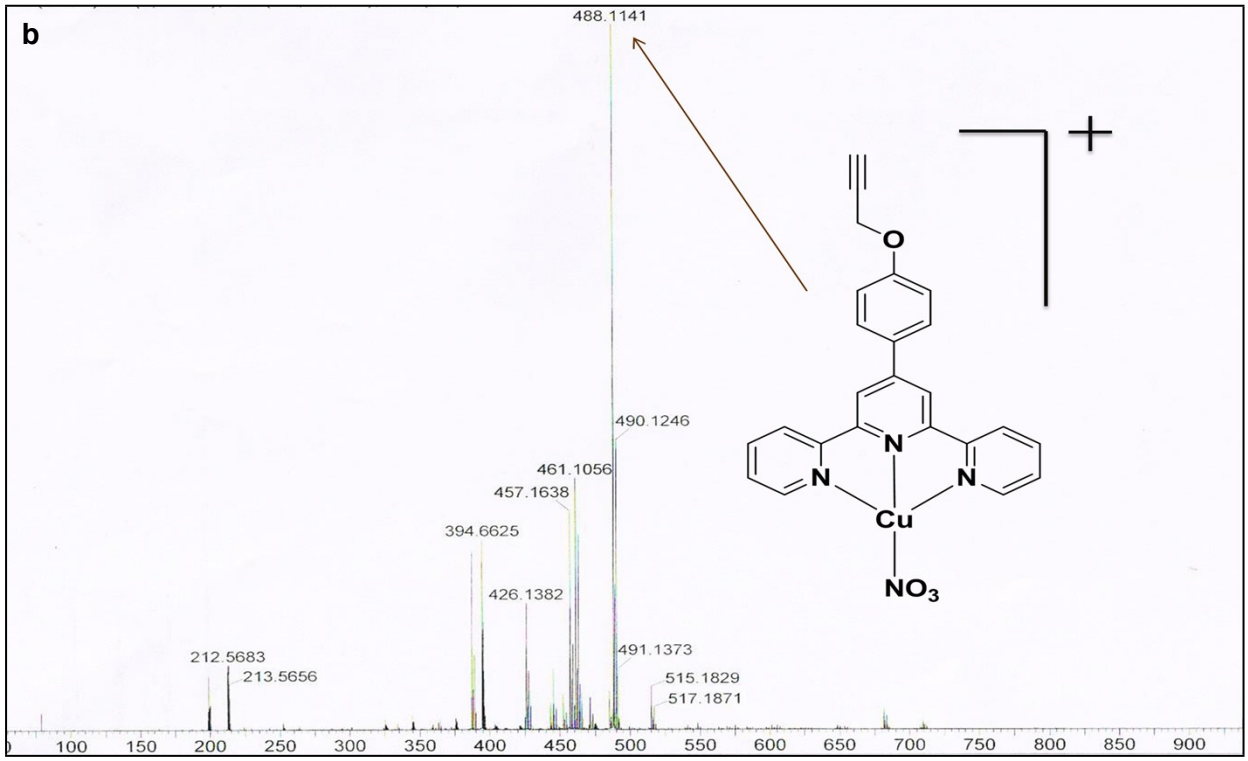

Figure S7. ESI- Mass spectra of (a) Ni-TRPA-2 and (b) Cu-TRPA-2

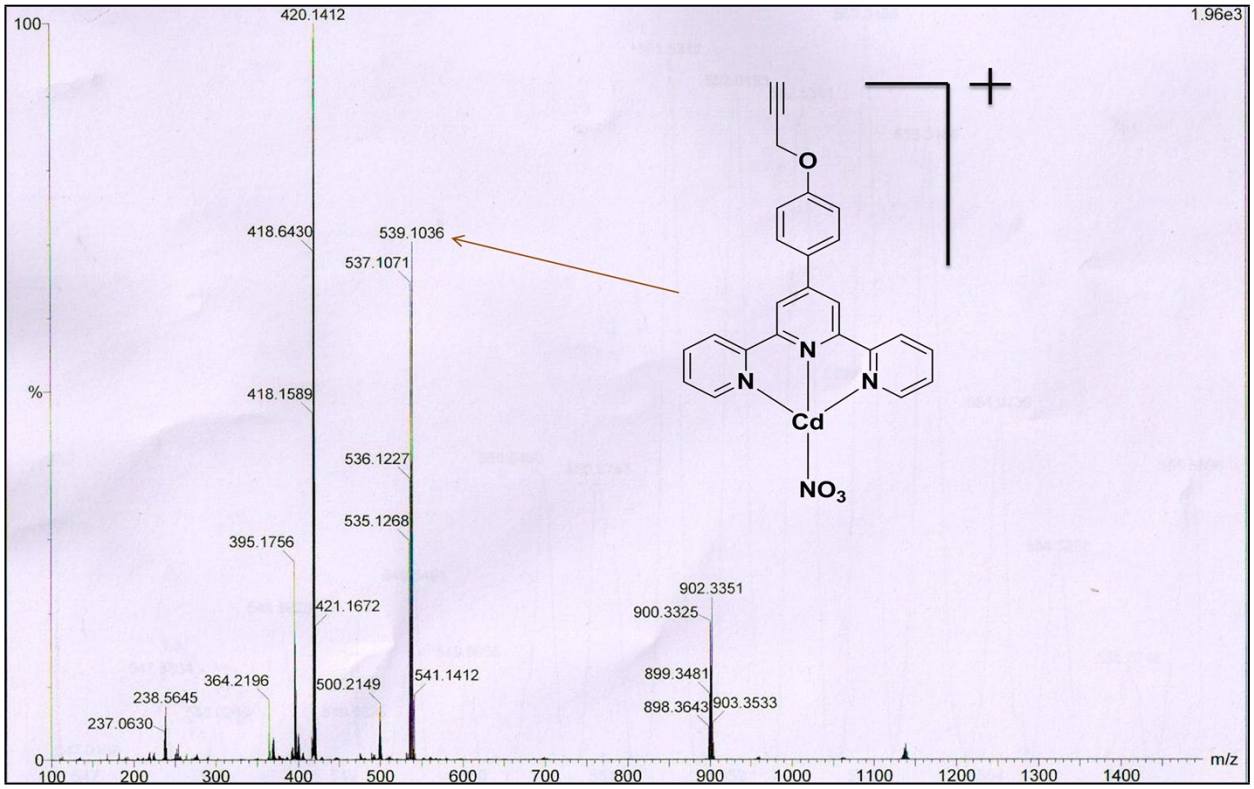

Figure S8. ESI- Mass spectra for Cd-TRPA-2

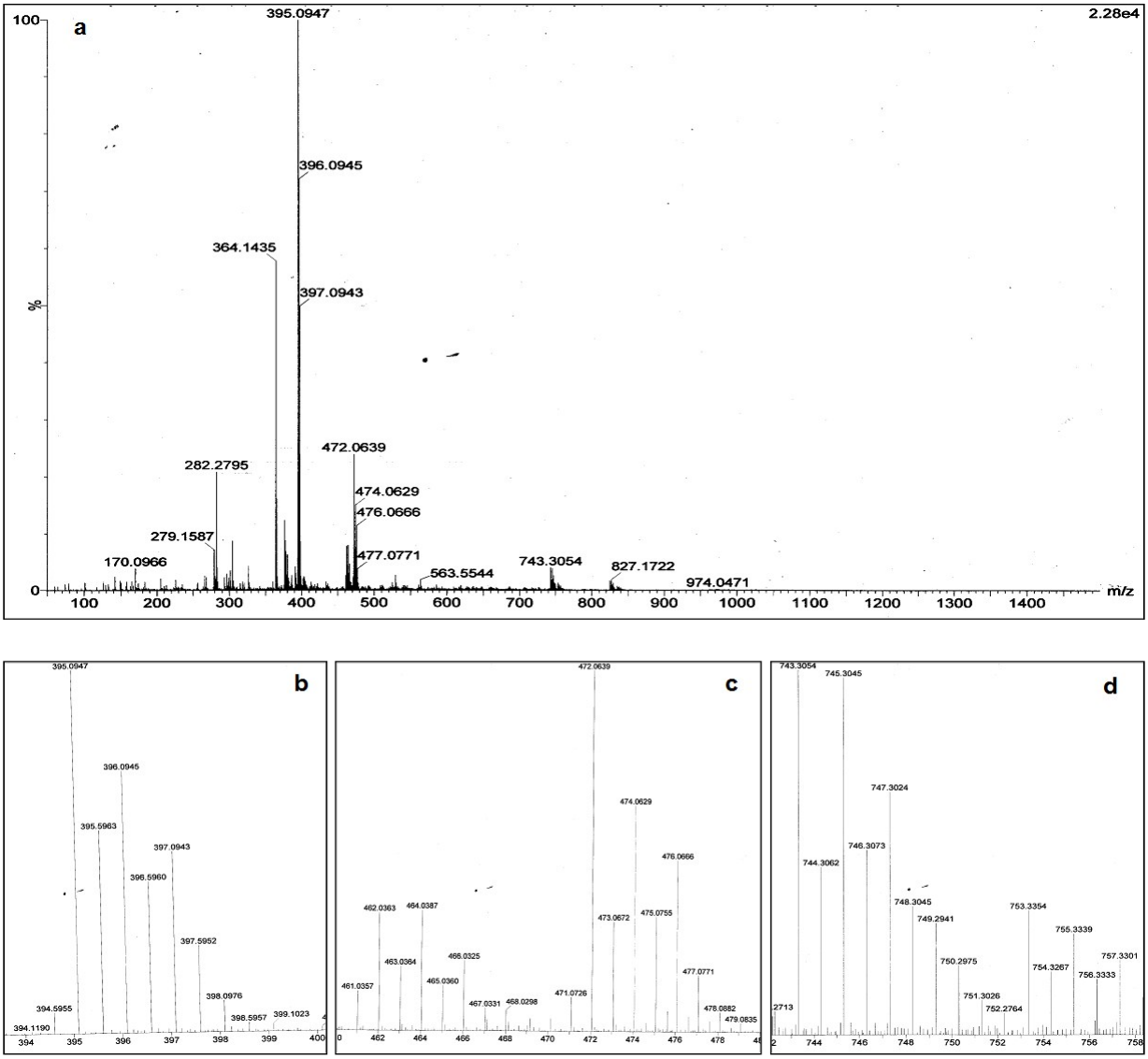

Figure S9. ESI- Mass Spectra of (a) dried ZTP2G along with (b, c & d) isotopic distribution of major peaks

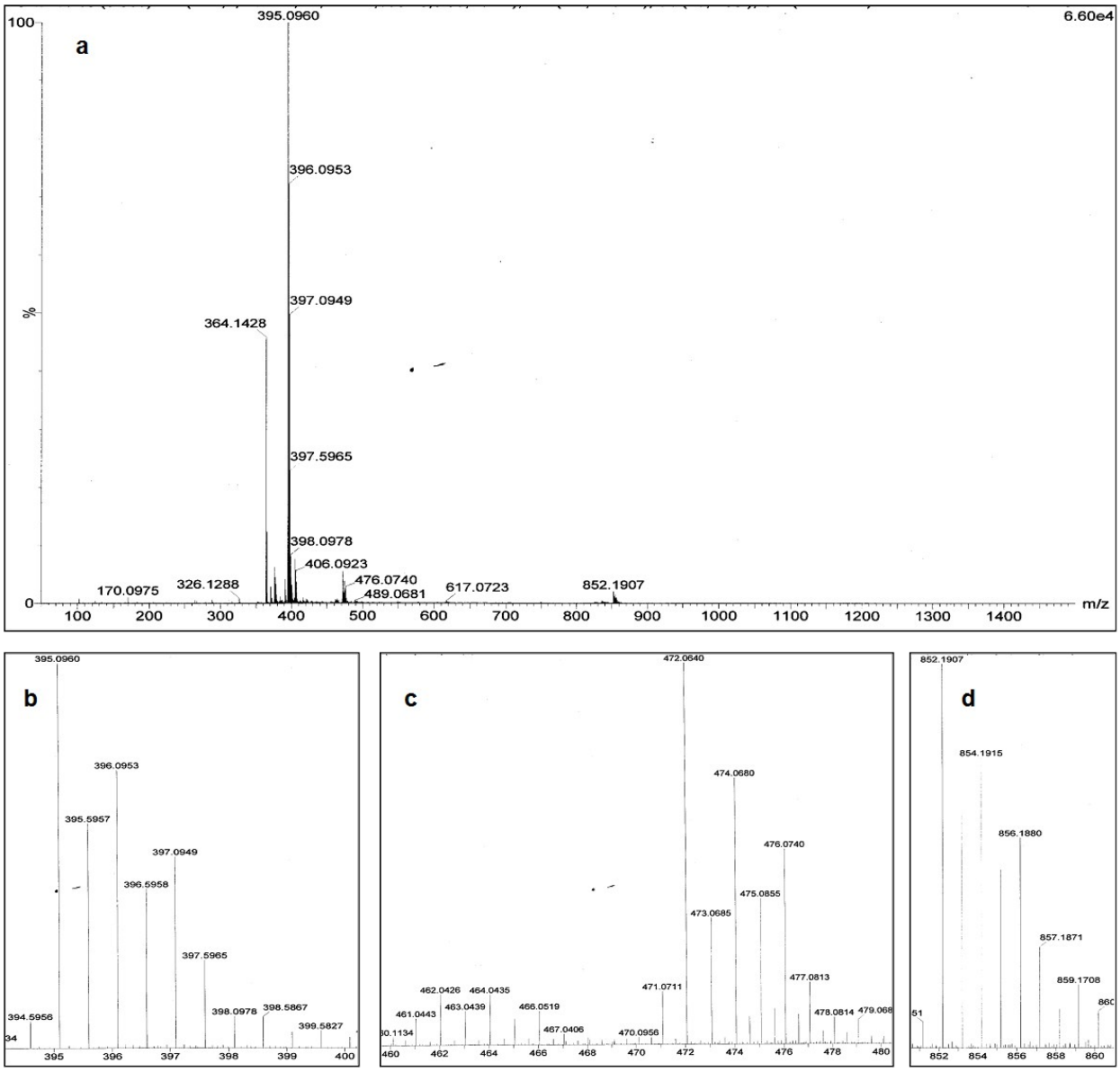

Figure S10. ESI- Mass Spectra of (a) crystalline NA-TRPA-2; (b, c & d) isotopic distribution of major peaks

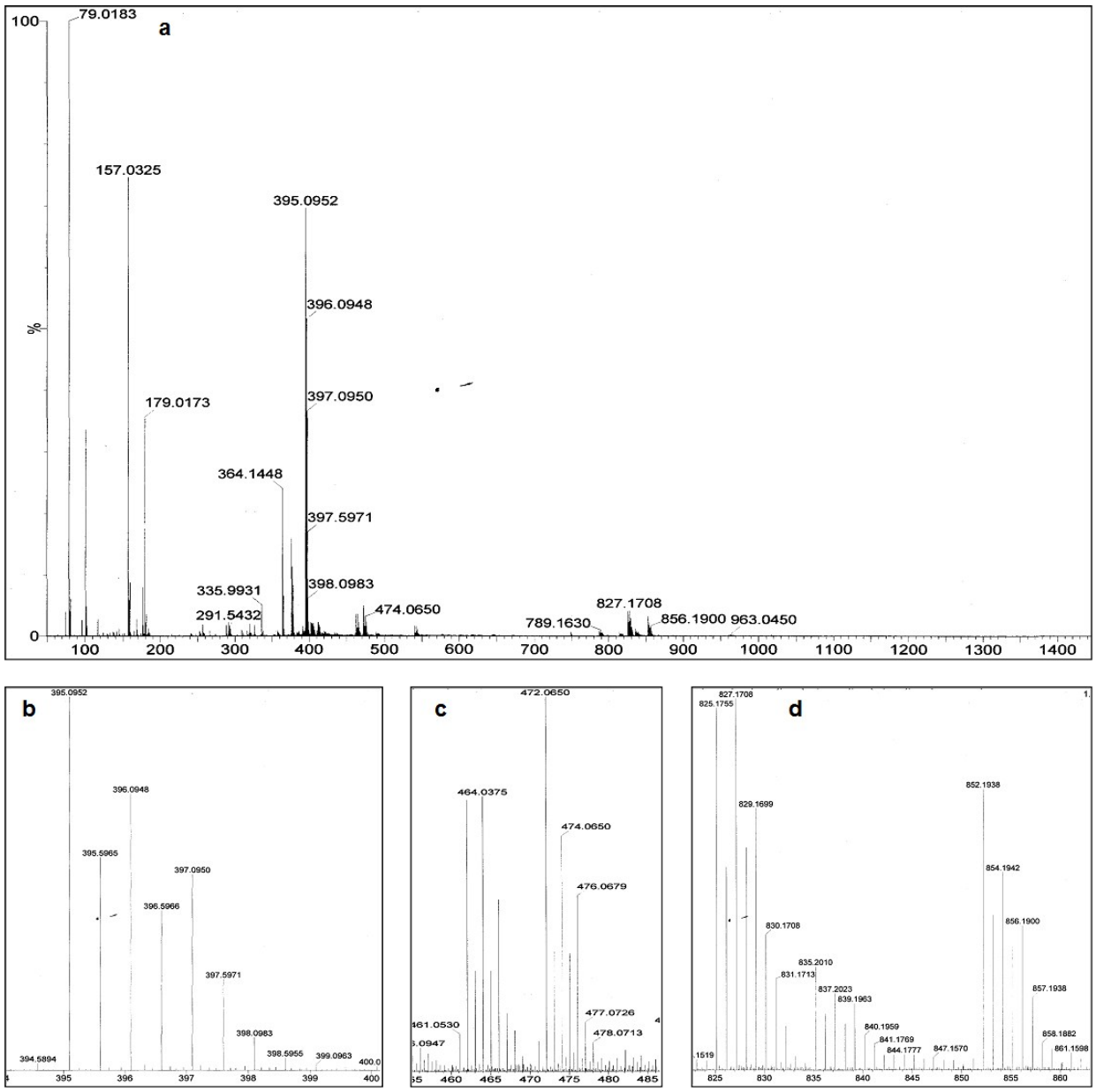

Figure S11. ESI- Mass spectra of (a) metallogel ZTP2G with crystals of NA-TRPA-2 inside; (b, c & d) isotopic distributions of the major peaks

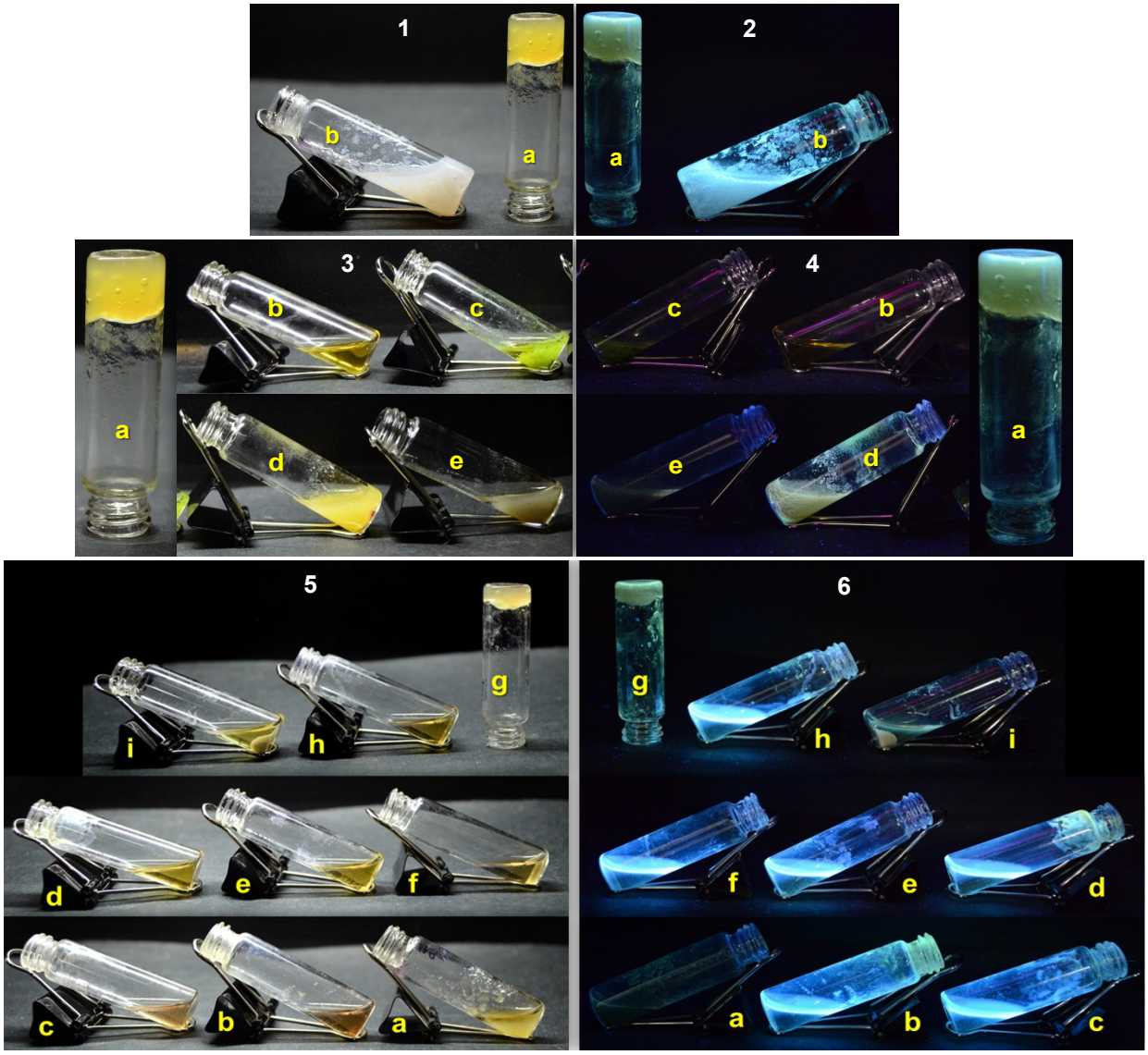

Figure S12. Comparative gelation experiments with (1) Isomers; (a) **TRPA-2** and (b) **TRPA-1** with Zn^{2+} (metal) and HCl (acid) under visible light. (2) Same under UV-light. (3) Metal complexes of **TRPA-2**; (a) Zn^{2+} (b) Ni^{2+} (c) Cu^{2+} (d) Cd^{2+} (e) Hg^{2+} with acid HCl under visible light. (4) Same under UV light. (5) Acids (a) HBr, (b) Oxalic acid ($H_2C_2O_4$), (c) Formic acid (HCO_2H), (d) H_2SO_4, (e) HNO_3, (f) Acetic acid (CH_3CO_2H), (g) HCl, (h) TFA (CF_3CO_2H), (i) $HClO_4$, with **Zn-TRPA-2** in methanol under visible light and (6) Same under UV light.

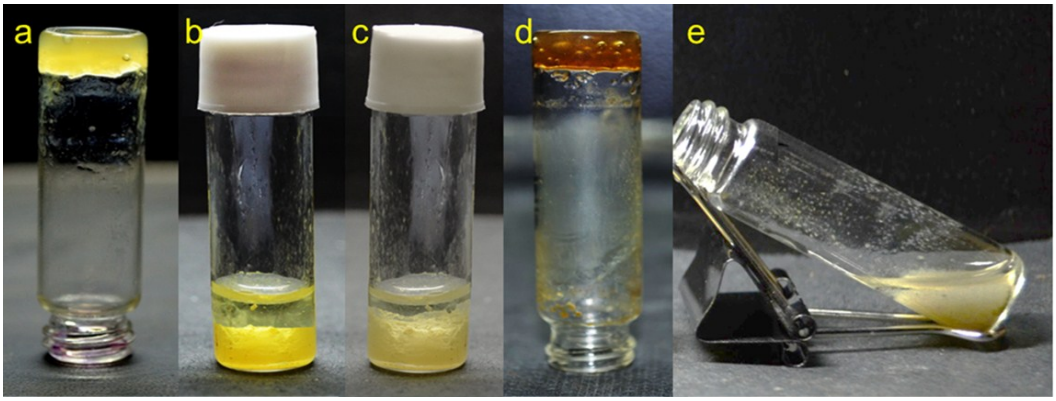

Figure S13 Images showing (a) metallogel ZTP2G, (b) unsuccessful trial for Au-NP incorporation after ZTP2G formation, (c) unsuccessful trial for Ag-NP incorporation after ZTP2G formation, (d) metallogel GNZTP2G as a result of successful incorporation of Au-NPs by triggering Zn-TRPA-2 capped Au-NPs by Cl^- (precisely HCl), (e) triggering Zn-TRPA-2 capped Ag-NPs by Cl- (profoundly HCl) could produce only a precipitate instead of a gel.

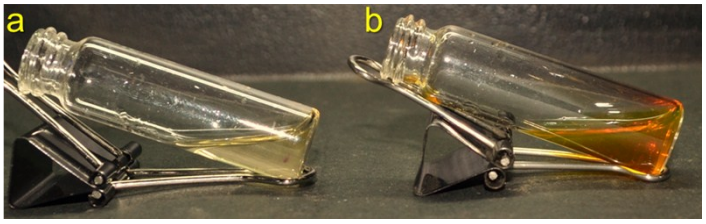

Figure S14 Images Showing that none of the ligands (a) TRPA-1 and (b) TRPA-2 forms a gel upon addition of 0.25M HCl under gelation conditions.

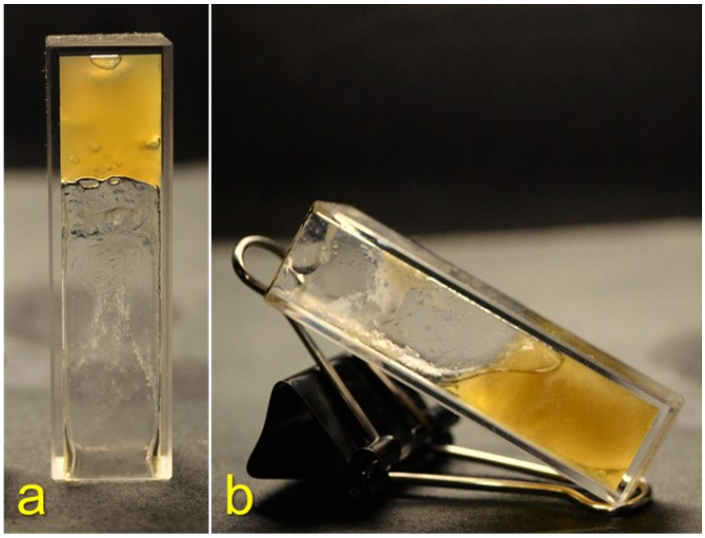

Figure S15 Effect of temperature on the gel ZTP2G: (a) at room temperature (30 ^{0}C, without heating) and (b) at room temperature after simultaneous heating to 90 ^{0}C and cooling.

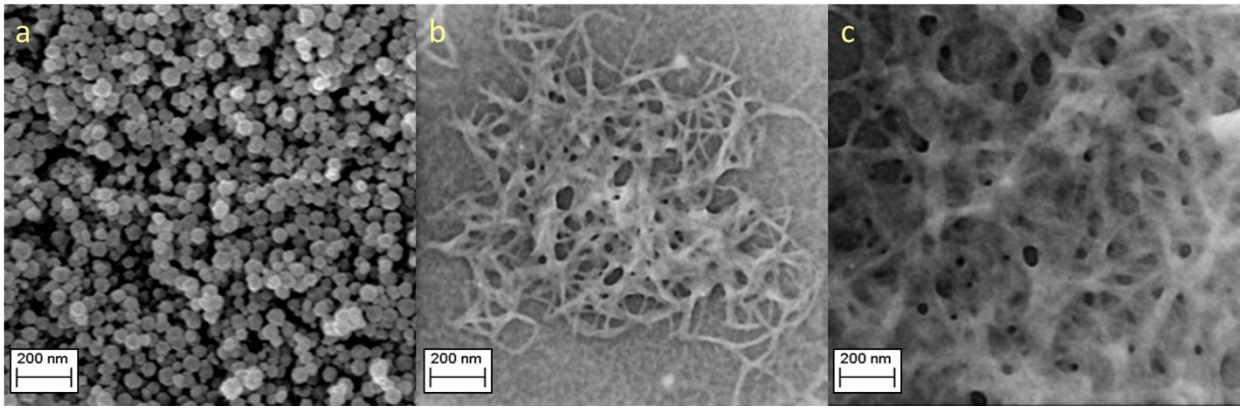

Figure S16. SEM images for (a) Gold Nanoparticles (Au-NPs) showing a regularly spherical shape which is in good agreement with TEM and AFM; (b) Metallogel ZTP2G showing fibrous morphology in accordance to TEM and AFM; (c) Metallogel GNZTP2G also revealed its fibrous morphology supporting to TEM and AFM.

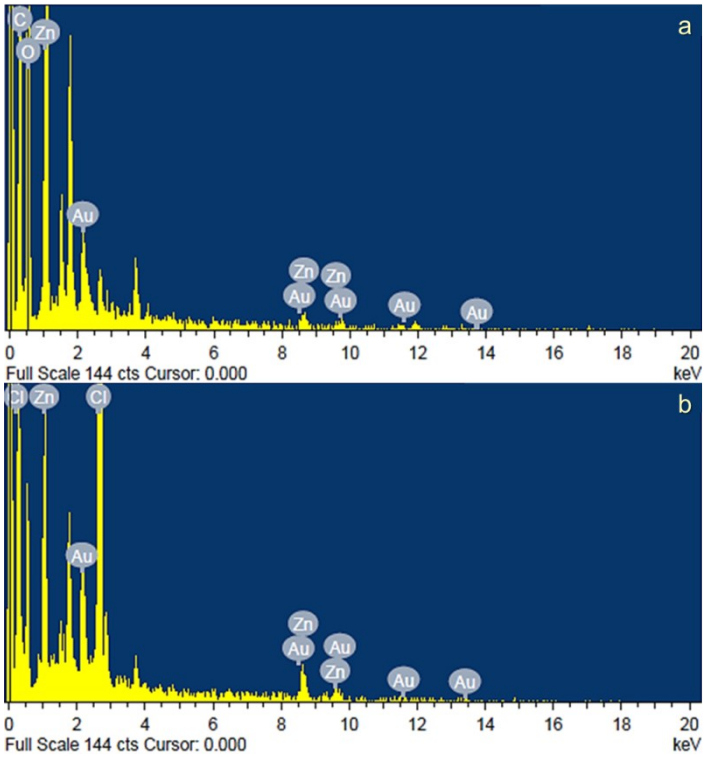

Figure S17. Energy Dispersive X-ray spectra for (a) Zn-TRPA-2 capped Au-NPs and (b) GNZTP2G convincingly showing the presence of Au/Zn in nanoparticle and that of Au/Zn/Cl in metallogel GNZTP2G. It has also been observed that a ratio of ~2:1 maintained in both Zn-TRPA-2 capped Au-NPs and GNZTP2G. This result not only suggested the heterobimetallogel formation, but also indicated that GNZTP2G fibers have been constructed by the capped NPs which is in good agreement with the TEM analysis as well.

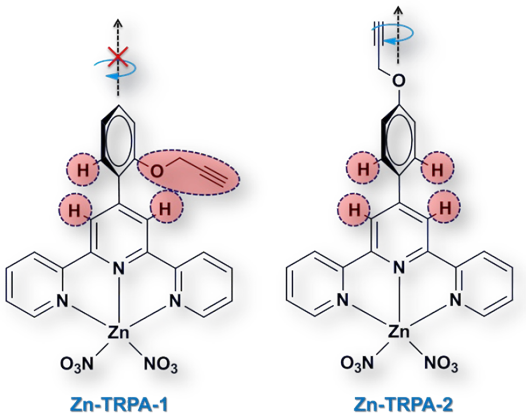

Figure S18. Structure elucidations of Zn-TRPA-1 and Zn-TRPA-2 revealed that the position of the prop-2-yn-1-yloxy chain which is closer to the terpyridyl moiety, restricts Zn-TRPA-1 to achieve planarity and thereby a stable gelation through π–π stacking whereas for Zn-TRPA-2 those can be achieved easily.

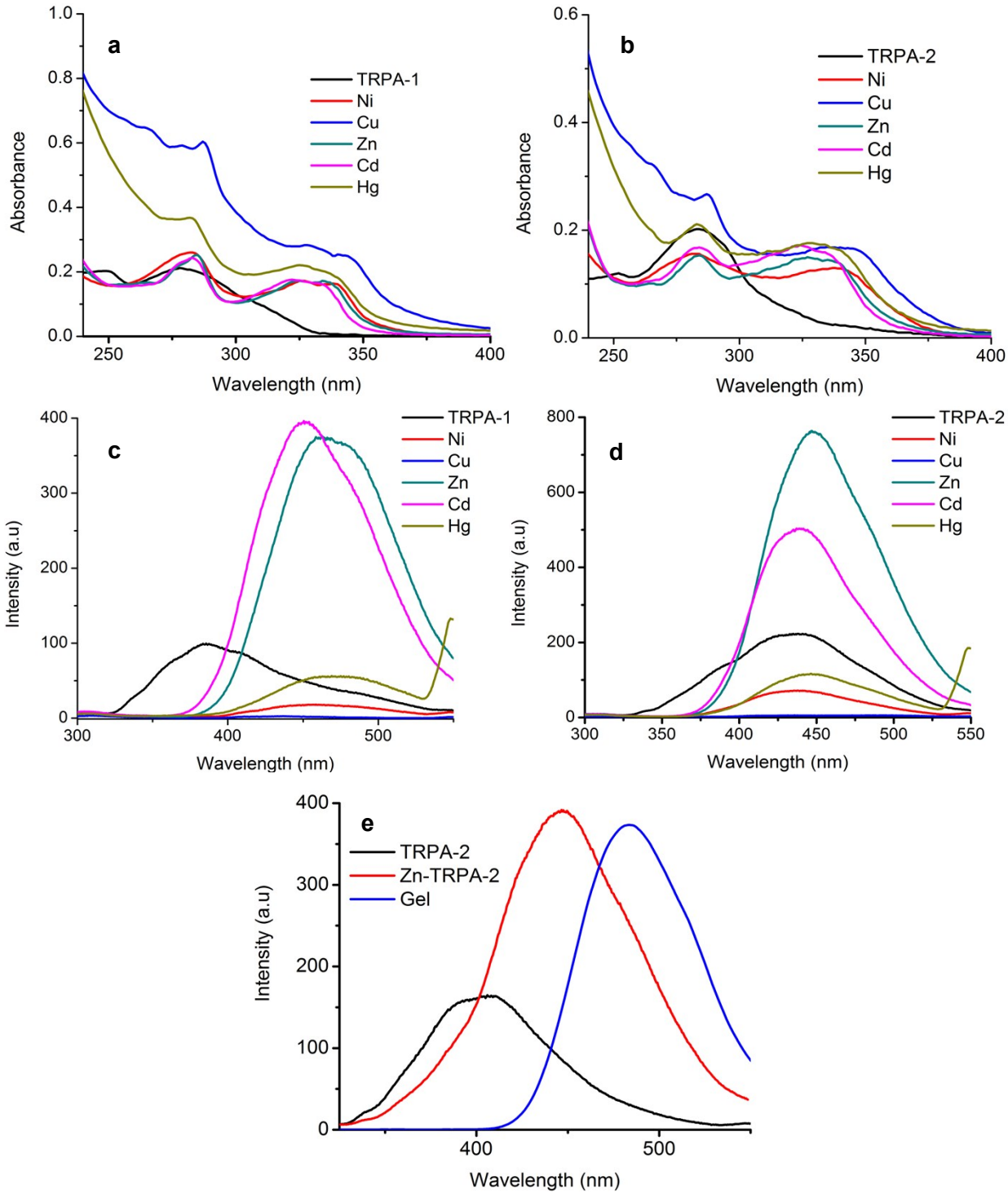
a
TRPA-1
Ni
Cu
Zn
Cd
Hg
Absorbance
Wavelength (nm)
b
TRPA-2
Ni
Cu
Zn
Cd
Hg
Absorbance
Wavelength (nm)
c
TRPA-1
Ni
Cu
Zn
Cd
Hg
Intensity (a.u)
Wavelength (nm)
d
TRPA-2
Ni
Cu
Zn
Cd
Hg
Intensity (a.u)
Wavelength (nm)
e
TRPA-2
Zn-TRPA-2
Gel
Intensity (a.u)
Wavelength (nm)

Figure S19. UV-vis spectra showing interaction of metal ions with (a) TRPA-1 and (b) TRPA-2; Fluorescence spectroscopic studies on metal ion interaction with (c) TRPA-1 and (d) TRPA-2; (e) Fluorescence spectra of ligand (TRPA-2), complex (Zn-TRPA-2) and gel (ZTP2G) showing red shifts during chelation (~60 nm) and gelation (~40 nm).

Table S1. UV-vis titration of TRPA-1/2 (Methanol) with Zn^{2+} (Methanol):

Ligand (10^{-5} M)	**Metal** (10^{-2} M)	**Peaks**		**Isosbestic point**
		n – π*; [ε ($mol^{-1}cm^{-1}$)]	ICT; [ε ($mol^{-1}cm^{-1}$)]	
TRPA–1	–	~280 nm; [1.19×10^5]	–	~307 nm
	0.2 equiv. Zn^{2+}	~280 nm; [1.20×10^5]	~340 nm; [1.77×10^4]	
	3.0 equiv. Zn^{2+}	~280 nm; [1.30×10^5]	~340 nm; [9.89×10^4]	
TRPA–2	–	~283 nm; [1.17×10^5]	–	~305 nm
	0.2 equiv. Zn^{2+}	~283 nm; [1.03×10^5]	~340 nm; [3.27×10^4]	
	2.0 equiv. Zn^{2+}	~283 nm; [7.12×10^4]	~340 nm; [8.92×10^4]	

Table S2. Fluorescence titration of TRPA-1/2 (Methanol) with Zn^{2+} (Methanol):

Ligand (10^{-5} M)	**Metal** (10^{-2} M)	**Ligand emission** (Intensity, au)	**New emission** (Intensity, au)	**Stokes shift**	**Isoemissive point**
TRPA–1	–	~385 nm; (211)	–	~90 nm	~307 nm
	0.2 equiv. Zn^{2+}	~385 nm; (194)	~475 nm; (92)		
	3.0 equiv. Zn^{2+}	~280 nm; (20)	~475 nm; (780)		
TRPA–2	–	~390 nm; (159)	–	~60 nm	~305 nm
	0.2 equiv. Zn^{2+}	~390 nm; (149)	~450 nm; (135)		
	2.0 equiv. Zn^{2+}	~390 nm; (83)	~450 nm; (780)		

Table S3. Variable Temperature Fluorescence spectra of ZTP2G

Temperature (^{0}C)	**Emission**	**Intensity (au)**
30	~480 nm	374
45	~478 nm	447
60	~470 nm	496
65	~480 nm	239
75	~480 nm	177
90	~480 nm	156

Table S4. UV-vis spectra for Zn-TRPA-2 capping of Ag-/Au-NPs

Metal solution (10^{-2} M)	**Zn-TRPA-2** (10^{-5} M)	**Peaks**		**Shift in SP band** ($\Delta\lambda_{SP}$)
		ICT; [ε ($mol^{-1}cm^{-1}$)]	SP band; [ε ($mol^{-1}cm^{-1}$)]	
Au	–	~340 nm; [4.60×10^4]	–	~15 nm Blue shift
	5 min	~340 nm; [4.60×10^4]	~524 nm; [2.73×10^3]	
	90 min	~350 nm; [4.89×10^4]	~510 nm; [2.72×10^4]	
	120 min	~350 nm; [4.89×10^4]	~509 nm; [2.72×10^4]	
Ag	–	~340 nm; [4.53×10^4]	–	~19 nm Blue shift
	5 min	~340 nm; [4.53×10^4]	~451 nm; [6.39×10^3]	
	90 min	~345 nm; [4.85×10^4]	~433 nm; [4.49×10^4]	
	120 min	~345 nm; [4.85×10^4]	~433 nm; [4.49×10^4]	

Table S5. Fluorescence spectra Zn-TRPA-2 capping of Ag-/Au-NPs

Metal solution (10^{-2} M, 1 equiv.)	**Zn-TRPA-2** (10^{-5} M)	**Emission band** (Intensity, au)
Au	–	~450 nm; (377)
	5 min	~450 nm; (163)
	90 min	~450 nm; (57)
	120 min	~450 nm; (57)
Ag	–	~450 nm; (416)
	5 min	~450 nm; (199)
	90 min	~450 nm; (70)
	120 min	~450 nm; (70)

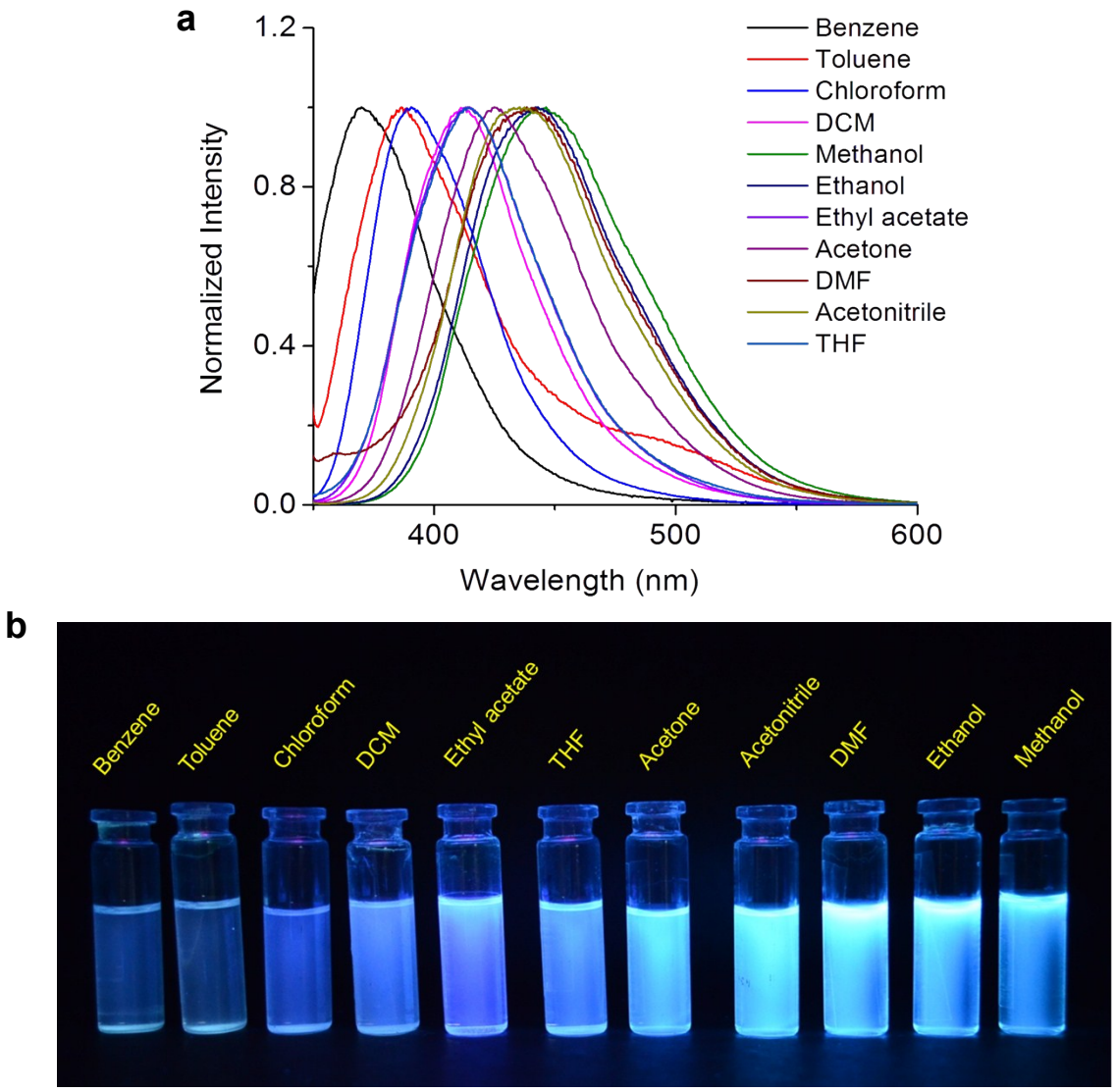

Figure S20. (a) A normalized fluorescence spectra showing a huge shift in the emission band of the complex Zn-TRPA-2 in various solvents viz. *benzene*, *toluene*, *chloroform*, *dichloromethane*, *ethyl acetate*, *tetrahydrofuran*, *acetone*, *acetonitrile*, *dimethylformamide*, *ethanol* and *methanol* (increasing polarity order). With increasing polarity the emission band which was appeared at 370 nm in benzene (most nonpolar) shifted to 450 nm in methanol (most polar) resulting a total shift of 80 nm. This fact accounted for a strong ICT in the Zn-complex. (b) Photograph showing the solvatochromism effect in Zn-TRPA-2 under UV-light.

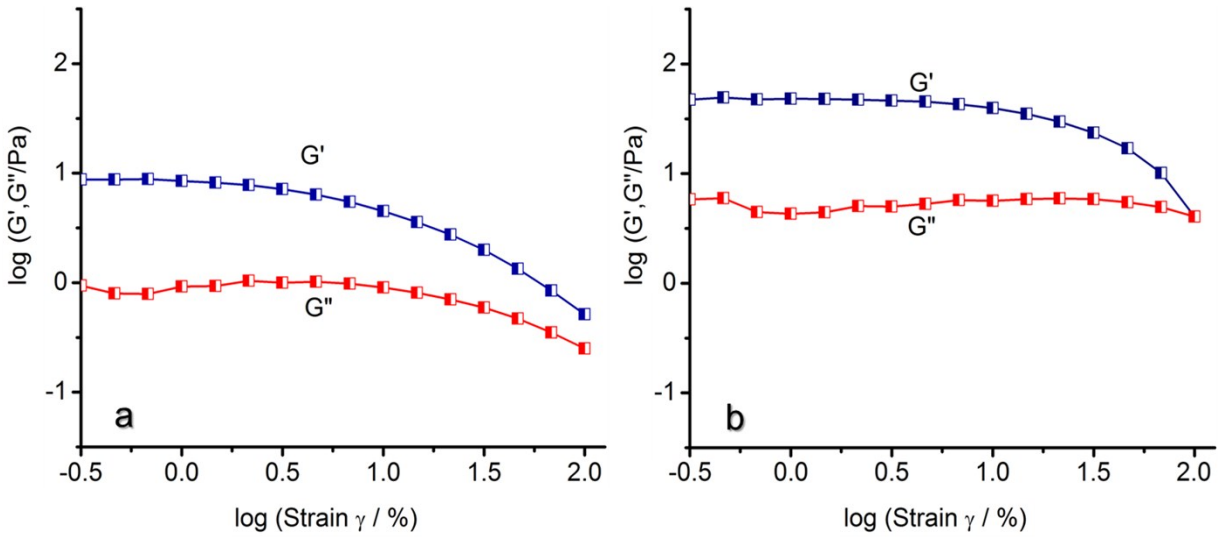

Figure S21. Logarithmic plot for oscillation strain (γ) sweep of storage (G') and loss (G'') modulus maintaining a characteristic difference of ~1 order between them for both (a) ZTP2G and (b) GNZTP2G. But at the same time it is also evident from the plots that both G' and G'' of GNZTP2G are considerably higher than those of ZTP2G.

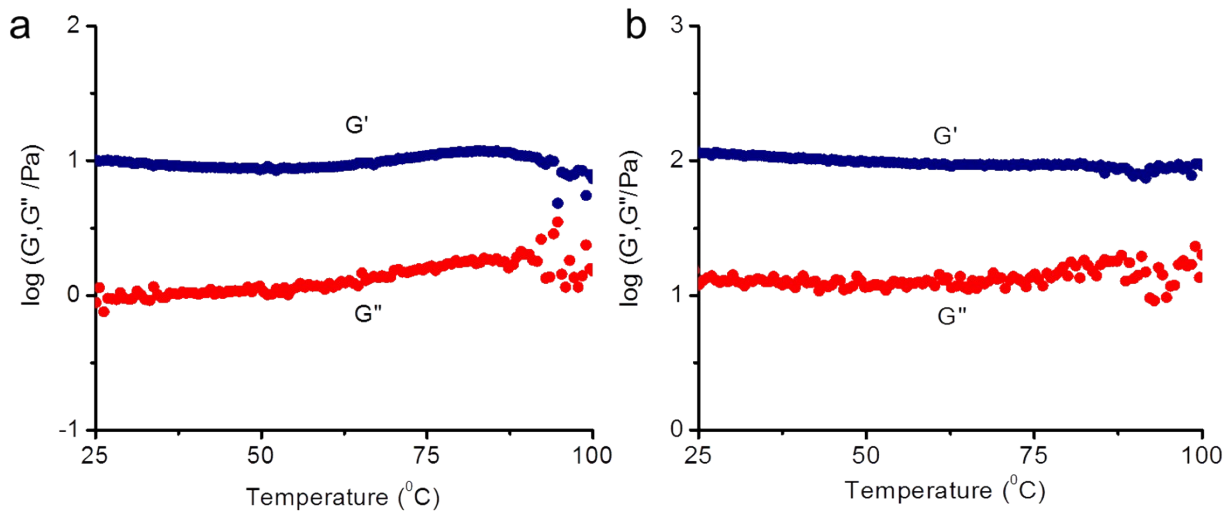

Figure S22. Dynamic temperature sweep of G' and G'' for (a) ZTP2G and (b) GNZTP2G.

Table S6. Unit cell parameters for the crystals of NA-TRPA-2

Crystallographic Data		**Crystal 1**	**Crystal 2**
Crystal System		Triclinic	Triclinic
Space group		'*P*-1'	'*P*-1'
Unit cell lengths (Å)	a	7.856(5)	8.089(6)
	b	11.799(7)	11.801(9)
	c	14.315(8)	14.428(11)
Unit cell angles (°)	α	66.980(14)	66.959(13)
	β	77.401(15)	77.200(15)
	γ	74.377(16)	74.252(14)
Unit cell volume (Å^3)		1166.7(12)	1209.4(15)
Temperature (K)		293	293

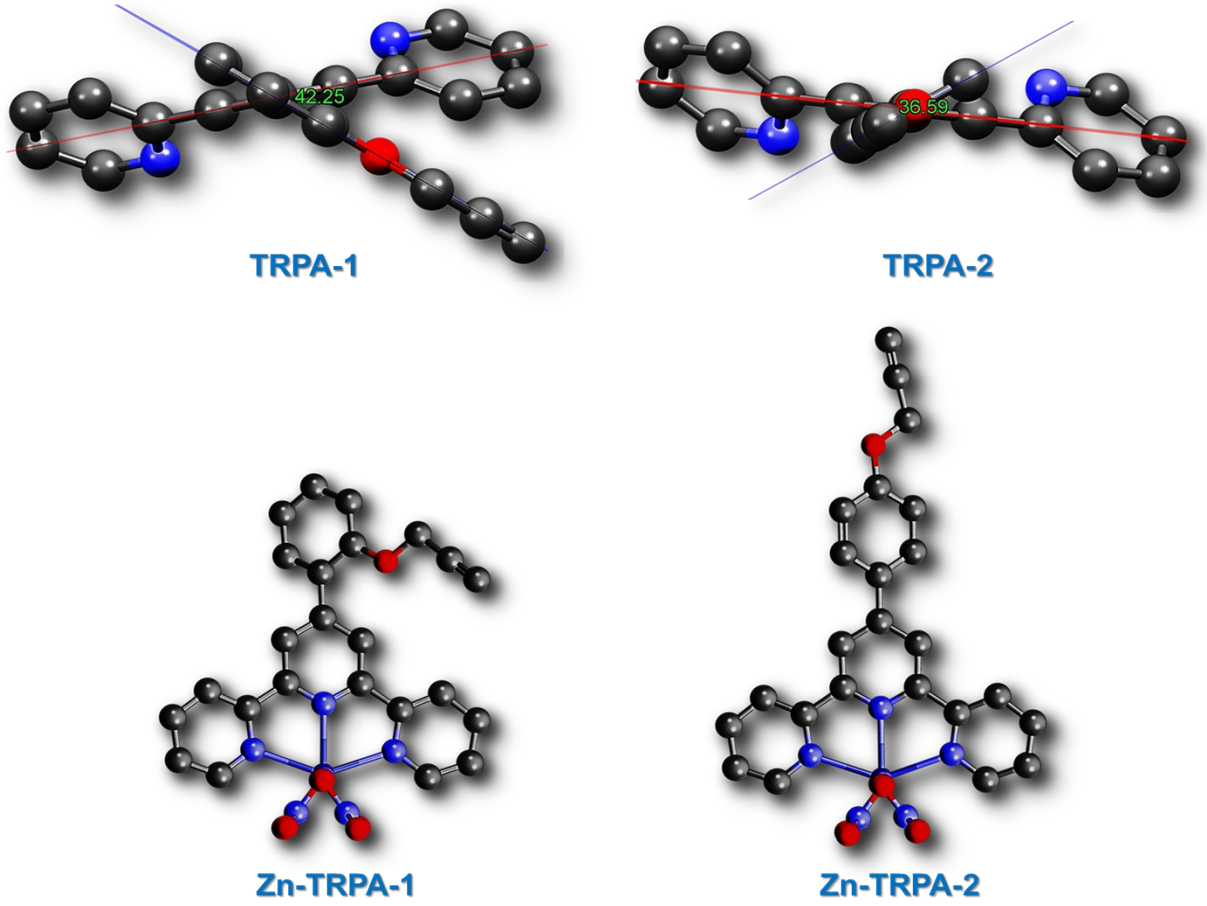

Figure S23. Theoretically optimized structures of ligands showing the dihedral angle between terpyridyl moiety and (prop-2-yn-1-yloxy)-phenyl unit is significantly higher in TRPA-1 (42.25^{o}) than that in TRPA-2 (36.59^{o}) indicating greater steric interaction in the former one. However none of the ligands have a

planar terpyridyl core. Again, optimized structures for complexes Zn-TRPA-1 and Zn-TRPA-2 revealed during complexation terpyridyl moiety attains planarity.

References:

1. G. M. Sheldrick *SHELXL-97: Program for Crystal Structures Refinement* University of Göttingen: Göttingen, Germany, 1997.
2. (a) A. L. Spek, *PLATON A Multipurpose Crystallographic Tools*, Utrecht University, Utrecht, The Netherlands, 2000. (b) A. L. Spek, *Acta Crystallogr. A*, 1990, **46**, C31. (c) L. J. Farrugia *J. Appl. Crystallogr*. 1999, **32**, 837.
3. L. J. Bartolottiand, K. Fluchick *Reviews in Computational Chemistry* 2007, **7**, 187.
4. P. Hay, W. R. Wadt *J. Chem. Phys.* 1985, **82**, 270; P. Hay, W. R. Wadt *J. Chem. Phys.* 1985, **82**, 284; P. Hay, W. R. Wadt *J. Chem. Phys.* 1985, **82**, 299.
5. M. J. Frisch, G. W. Trucks, H. B. Schlegel, G. E. Scuseria, M. A. Robb, J. R. Cheeseman, G. Scalmani, V. Barone, B. Mennucci, G. A. Petersson, H. Nakatsuji, M. Caricato, X. Li, H. P. Hratchian, A. F. Izmaylov, J. Bloino, G. Zheng, J. L. Sonnenberg, M. Hada, M. Ehara, K. Toyota, R. Fukuda, J. Hasegawa, M. Ishida, T. Nakajima, Y. Honda, O. Kitao, H. Nakai, T. Vreven, J. A. Jr. Montgomery, J. E. Peralta, F. Ogliaro, M. Bearpark,; J. J. Heyd, E. Brothers, K. N. Kudin, V. N. Staroverov, R. Kobayashi, J. Normand, K. Raghavachari, A. Rendell, J. C. Burant, S. S. Iyengar, J. Tomasi, M. Cossi, N. Rega, N. J. Millam, M. Klene, J. E. Knox, J. B. Cross, V. Bakken, C. Adamo, J. Jaramillo, R. Gomperts, R. E. Stratmann, O. Yazyev, A. J. Austin, R. Cammi, C. Pomelli, J. W. Ochterski, R. L. Martin, K. Morokuma, V. G. Zakrzewski, G. A. Voth, P. Salvador, J. J. Dannenberg, S. Dapprich, A. D. Daniels, Ö. Farkas, J. B. Foresman, J. V. Ortiz, J. Cioslowski and D. J. Fox, *Gaussian 09, revision A.1* Gaussian, Inc.: Wallingford, CT, 2009.